Nonlinear Behavior and Bias Modulation of an IMPATT Diode Oscillator

CHENTE CHAO AND GEORGE I. HADDAD

Abstract—**Experimental results of the nonlinear behavior of an IMPATT diode oscillator under free-running and bias-modulated conditions are presented and correlated with theoretical results. Amplitude and frequency behavior of a free-running IMPATT diode oscillator such as: 1) power-frequency characteristic, 2) jump and hysteresis, 3) temperature dependence, 4) harmonic content, and 5) electronic tuning characteristics are discussed. The bias-modulation properties and their relation to the free-running behavior are described. The effects of the operating point, external Q, and injection locking on the modulation properties are presented.**

I. Introduction

THE IMPATT diode has reached an advanced state of development and is presently being employed in several applications. Several review papers [1], [2] are available where the basic principles of operation, the device physics, methods of fabrication and characterization, and modes of operation are presented. More recent work in the field has been focused on the nonlinear properties of these devices [3] and the problems which can arise during operation [4]. The purpose of this paper is, therefore, to present the nonlinear operating characteristics of these devices and to describe the interaction between the device and the circuit.

In Section II, the nonlinear behavior of a free-running IMPATT diode oscillator is presented along with a theoretical explanation. The behavior of a bias-modulated IMPATT diode oscillator is presented in Section III. The effects of the operating point, external Q and injection locking on the modulation properties are described and compared with the theoretical expression. The emphasis is placed on a correlation between theory and experiment concerning the behavior of a negative-resistance diode oscillator in terms of the device-circuit interaction.

II. Behavior of a Free-Running Oscillator

In the study of an IMPATT diode oscillator, an understanding of the free-running behavior is essential to its performance in a system application. In the course of a routine tuning experiment, for example, some nonlinear phenomena are often observed that cannot be explained by a simple oscillator model. Among them the commonly observed ones include the following.

1) The frequency and power of the oscillator exhibit a discontinuous change or "jump" as the dc bias current or the circuit tuning element is varied. If the tuning is reversed, the jump occurs at a different frequency and power. This is referred to as a "hysteresis" effect.

2) As the temperature of the heat sink changes, the power and frequency of the oscillator also change even though the dc bias current and the external circuit are fixed.

3) Under certain bias-circuit configurations, such as modulating the dc bias current of the diode through a capacitor or a transformer or detecting the Doppler-shifted frequency in a Doppler-type radar application, the additional circuitry incorporated in the bias network may give rise to low-frequency oscillations which create sidebands and/or modulation in the single-line spectrum. Such low-frequency bias-circuit oscillations will disappear only if the dc bias current level and/or bias circuit are changed. This is in agreement with the recent work of Brackett [5]. In his paper it was shown that these instabilities may be eliminated in a systematic and well-controlled manner.

4) Excess noise or sideband generation may occur near a frequency jump or under certain operating conditions.

The behavior of an IMPATT diode oscillator depends on the properties of the circuit employed and the device. A precise knowledge of the circuit and device properties of an oscillator will allow one to predict its behavior under various operating conditions and to gather valuable information to aid in its optimum design. The behavior of a negative-resistance diode oscillator is adequately explained in terms of the device and circuit interaction. In order to achieve this, an appropriate model of the oscillator and reasonably accurate methods of calculating the circuit and device impedances must be available. Recently, a systematic analysis of the negative-resistance diode oscillator was treated by Kurokawa [6]. In his paper, the condition for free-running stable oscillations, injection-locking phenomena, stable-locking range, noise of free-running and injection-locked oscillators, and a condition for parasitic oscillations were discussed analytically and graphically in terms of the device-circuit interaction. Some of his results were verified experimentally in a low-frequency lumped circuit by Kenyon [7].

When a device with an admittance $Y_d = -G_d + jB_d$ is connected to a passive circuit whose admittance is $Y_c = G_c + jB_c$, the voltage amplitude V and frequency ω of the resulting steady-state oscillation are determined by

$$\begin{aligned} G_d(V, \omega) - G_c(\omega) &= 0 \\ B_d(V, \omega) + B_c(\omega) &= 0. \end{aligned} \tag{1}$$

These equations are the conditions for oscillation and define the intersection in the complex admittance plane of the loci $Y_c(\omega) = G_c(\omega) + jB_c(\omega)$ and $-Y_d(V, \omega) = G_d(V, \omega) - jB_d(V, \omega)$.

Stable oscillation is possible if and only if, in addition to the condition for oscillation (1), the following stability requirement is fulfilled at each intersection in the admittance plane plot:

$$-V \frac{\partial G_d}{\partial V} \frac{dG_c}{d\omega} (\tan \Theta - \tan \theta) > 0 \tag{2}$$

Manuscript received February 8, 1973; revised May 24, 1973. This work was supported in part by the Highway Safety Research Institute, University of Michigan, Ann Arbor, and Omni Spectra, Inc., Farmington, Mich.

The authors are with the Department of Electrical and Computer Engineering, Electron Physics Laboratory, University of Michigan, Ann Arbor, Mich. 48104.

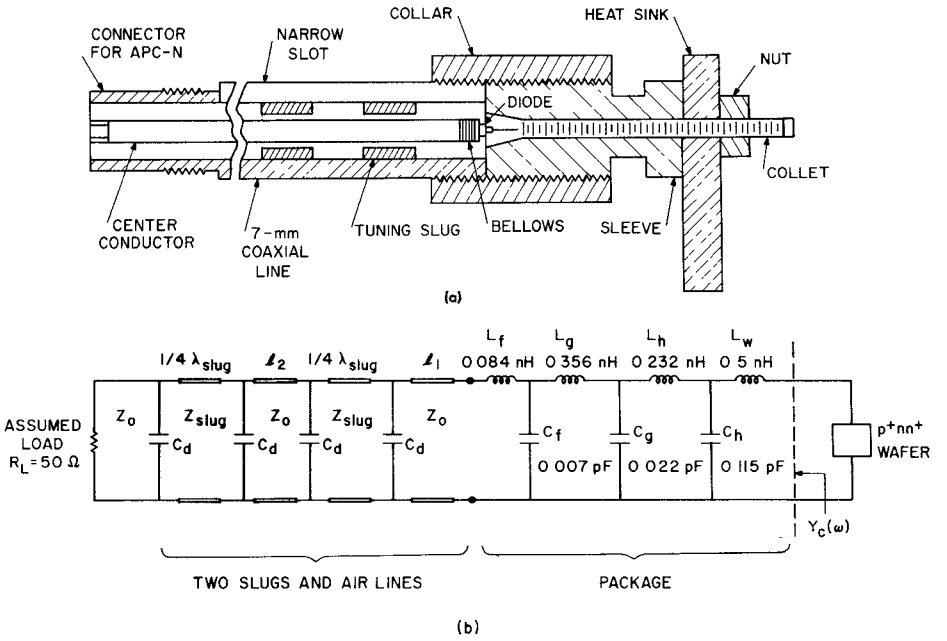

Fig. 1. (a) Cross section of the coaxial cavity. (b) Equivalent circuit of the diode package and slugs ($C_d = 86.2 \times 10^{-15}$F, $Z_0 = 50\ \Omega$, $Z_{slug} = 10\ \Omega$).

where

$$\tan \Theta = \frac{\dfrac{dB_c}{d\omega}}{\dfrac{dG_c}{d\omega}}$$

and

$$\tan \theta = \frac{\dfrac{\partial B_d}{\partial V}}{\dfrac{\partial G_d}{\partial V}}.$$

For a device which is biased through a constant-current source, it is preferred to analyze the device-circuit interaction on an admittance plane instead of on an impedance plane. The reason is explicitly implied by the factor $\partial G_d/\partial V$ in (2) which is the derivative of device conductance with respect to RF voltage across the device along a constant-current locus. On the other hand, it is preferable to work on an impedance plane for a device, for example, transferred-electron device, which is biased by a constant-voltage source.

In this section, some experimental data on the nonlinear behavior of a free-running IMPATT diode oscillator will be presented. The conditions for oscillation and the stability criterion, (1) and (2), respectively, are used to analyze the data.

A. Diode Model

The diodes which were used in the experimental work and all subsequent analyses are made of Si and have a p^+-n-n^+ doping profile. The doping density in the n-region was determined to have an average value of 7.5×10^{15} cm^{-3} by a measurement of the diode capacitance versus the reverse bias voltage. The acceptor concentration in the p^+-region is approximately 3×10^{19} cm^{-3}. The width of the n-region and the area of the diode are typically 4 μm long and 1×10^{-4} cm^2, respectively.

An approximate large-signal analysis is employed to calculate the impedance of the device. This model neglects the diffusion term in the current density equation and assumes that the holes and electrons have equal ionization rates and move at equal and saturated drift velocities. The diode is idealized to have an effective avalanche region 1 μm long and an effective drift region of 4 μm. The shape of the electric field profile in the avalanche region is assumed to be independent of time, but its magnitude is a function of time. Such a model has been used successfully by Blue [8] and Schroeder and Haddad [9] and provides a realistic description of an IMPATT diode.

B. Circuit Model

The oscillator consists of a Si p^+-n-n^+ diode in an HP 41 package which is mounted in a 7-mm coaxial line with two 10-Ω tuning slugs a quarter-wavelength long at various frequencies in X band. The cross section of the coaxial cavity and the equivalent circuit which was used in the calculation of the circuit impedance are shown in Fig. 1. A computer program was developed to calculate the circuit impedance as a function of frequency with the slug positions (l_1 and l_2) and the size of the slugs (λ_{slug} and Z_{slug}) as input parameters.

C. Experimental Results and Discussion

Power-Frequency Characteristics: The Si diode and the coaxial cavity described earlier were employed with other microwave components for studying the basic characteristics of these diodes as solid-state negative-resistance oscillators. In order to study the frequency range where the conditions for oscillation and stability are fulfilled, the diode was biased at a constant dc current and the position of the two tuning slugs was varied until a single-frequency clean spectrum at a reasonable power level was obtained. An example of such a power-frequency characteristic of a Si diode at a constant dc current of 80 mA and with the heat sink at ice water tem-

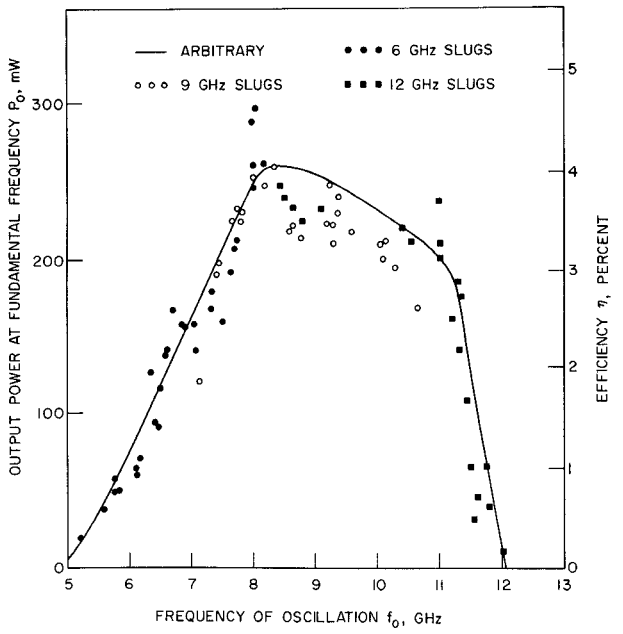

Fig. 2. Output power and efficiency versus frequency of oscillation for an IMPATT diode biased at a constant dc current of 80 mA in a coaxial cavity with two 10-Ω slugs a quarter-wavelength long at 6, 9, and 12 GHz, respectively.

perature (17°C) is shown in Fig. 2. Tuning slugs of different lengths were used to satisfy the condition of oscillation for different frequency ranges. For the data shown in Fig. 2, two identical slugs that were a quarter-wavelength long at 6, 9, and 12 GHz were used each time. One set of slugs can cover a range of frequency of more than 3 GHz. Oscillation at a higher frequency than the one shown in Fig. 2 (i.e., 12 GHz) can be obtained if slugs which are a quarter-wavelength long at a higher frequency are used. This is evident from the numerical simulation of the device impedance which exhibits a negative resistance at frequencies far beyond X band (Fig. 3). Thus, it is quite often due to an inadequate circuit impedance that the condition of oscillation is not satisfied. On the other hand, the theoretical prediction of a cutoff frequency near 6 GHz should not be taken literally since its calculation, in addition to the assumptions described earlier, is assumed to be at room temperature. The actual junction temperature can be as high as 250°C. At higher operating temperatures, the avalanche or cutoff frequency decreases with temperature due to the temperature dependence of the saturated drift velocity [10] and the ionization rate [11]. The observed oscillations below 6 GHz give additional evidence to the temperature dependence of these basic parameters. The effect of temperature on the performance of the IMPATT diode oscillator will be presented in a later section.

Jump and Hysteresis in Frequency and Power: The variation of frequency and power of the IMPATT diode oscillator with the dc bias current, when the external circuit is fixed, is referred to as the electronic tuning effect which was first described through a small-signal analysis by Gilden and Hines [12] and which provides a convenient way to modulate the oscillator. For certain operating conditions, the frequency and power of the IMPATT diode oscillator may vary smoothly over a wide range of the dc bias current (for example, see Fig. 4). However, for other operating conditions, a discontinuous change of frequency and power occurs when the dc bias current is varied. If the current tuning is reversed, the

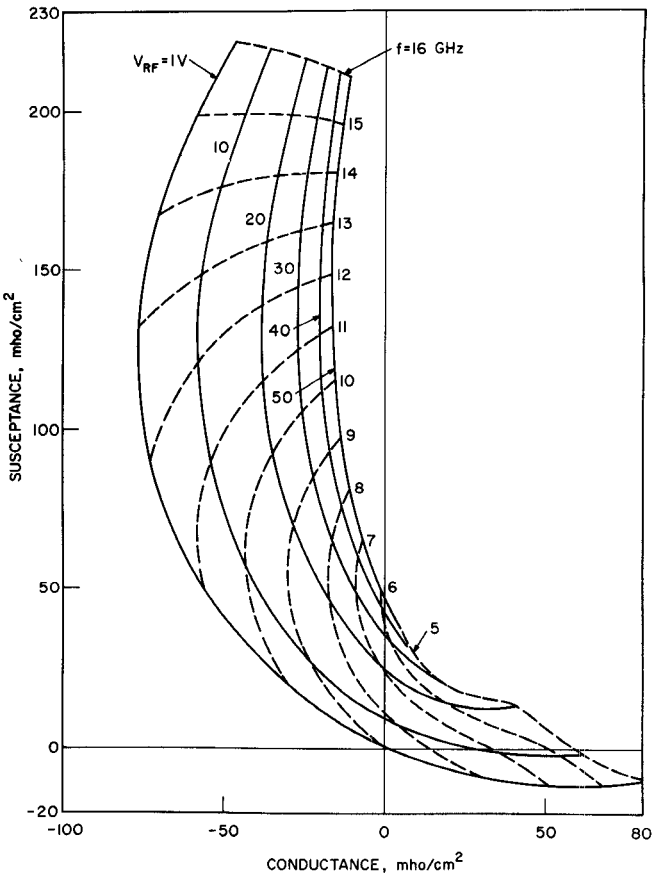

Fig. 3. Admittance of a Si p^+-n-n^+ diode as a function of RF voltage and frequency at a constant dc current density of 800 A/cm^2.

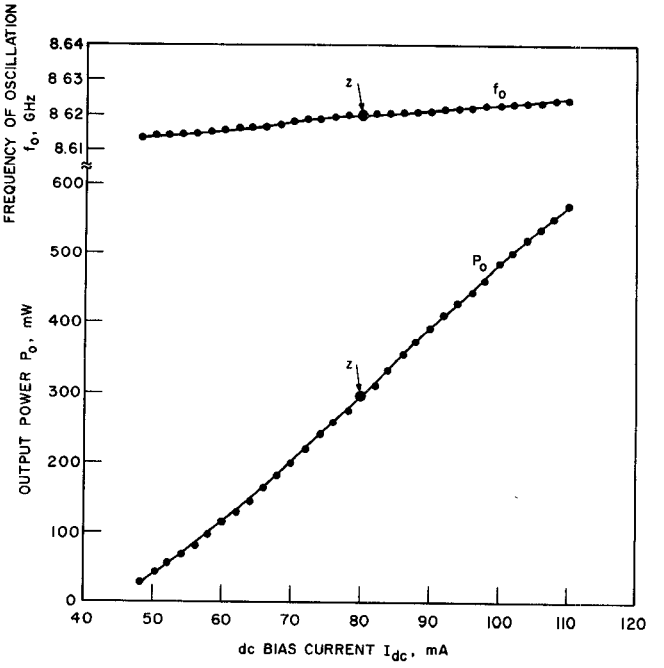

Fig. 4. Frequency of oscillation and output power versus dc bias current for a fixed external circuit. Point z was chosen as an operating point for studying the modulation properties of a bias-modulated IMPATT diode oscillator in Section III.

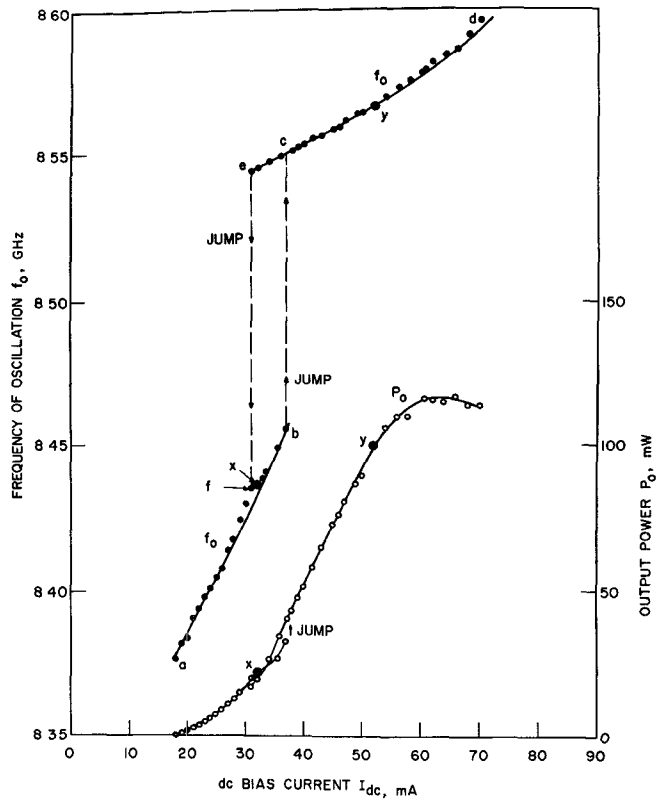

Fig. 5. Frequency of oscillation and output power versus dc bias current for a fixed external circuit. Points x and y were chosen as operating points for studying the modulation properties of a bias-modulated IMPATT diode oscillator in Section III.

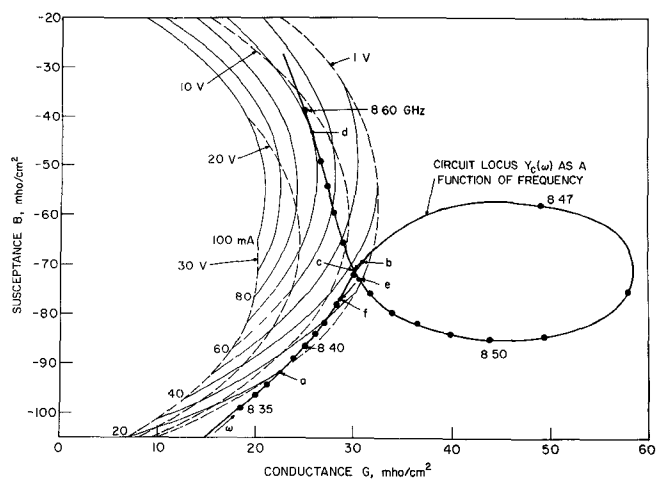

Fig. 6. Admittance plane plot of the circuit and device for the experimental data in Fig. 5.

discontinuity or jump occurs at a different value of frequency, power, and dc bias current. Thus there is a hysteresis loop with a jump in the frequency and power as a function of the dc bias current (see, for example, Fig. 5).

As an example, the jump and hysteresis shown in Fig. 5 are analyzed by superimposing the admittance of the device and circuit on an admittance plane plot (Fig. 6). The negative value of the device admittance at the fundamental frequency of oscillation as a function of bias current for different values of the RF voltage is plotted with the admittance of the circuit which varies as a function of frequency near the neighborhood of the frequency of oscillation. The calculation of the device admittance is based on the model described earlier. The dependence of the device impedance at the fundamental frequency due to the presence of harmonics is neglected since measurements of the harmonic content for the coaxial IMPATT diode oscillator (which shall be discussed later in this section) indicate that the second harmonic is usually the strongest one but is normally at a value of 20 dB below the power of the fundamental frequency. The effect of second harmonic on the device admittance at the fundamental frequency was illustrated systematically by Schroeder and Haddad [9]. It has been shown that there is negligible change in device admittance at the fundamental frequency due to the presence of a second harmonic at a level as low as 20 dB below the fundamental power for all values of phase between them. The dependence of the device admittance on the frequency is also neglected since there is a negligible change in the device admittance due to a small frequency change near an operating point.

The calculation of the circuit admittance is based on the equivalent circuit [13], [14] for the diode package and the actual position of the slugs as shown in Fig. 1. Two 10-GHz slugs are used, and the actual position of the slugs are $l_1 = 0$ cm and $l_2 = 1.75$ cm. The locus of the circuit admittance forms a loop near the frequency of interest and overlaps partially with the device admittance. A minor adjustment in the size of the loop of the circuit admittance has been made for the one shown in Fig. 6 which gives an excellent account of the jump and hysteresis observed in Fig. 5.

The reason for the jump and hysteresis which were observed experimentally is due to the combined effects that a loop exists in the locus of the circuit admittance which partially overlaps the device admittance and the requirements of the conditions for oscillation and stability. Stable oscillation can be maintained only if both the conditions for oscillation and the stability criterion are satisfied simultaneously at a given point of interest in the admittance plane.

A detailed account of the observed jump and hysteresis in frequency and power which are shown in Fig. 5 is given. The points of interest in the data shown in Fig. 5 are similarly labeled on the corresponding device-circuit admittance plot (Fig. 6) and in Fig. 7. At point a, the loci of the circuit and device begin to intersect, and the stability criterion is satisfied. As the dc bias current is increased the constant-current device lines move upward and are nearly parallel to one another. The frequency is increased as the intersection is moved upward until it is at point b beyond which the condition of stability is no longer satisfied and the jump from point b to point c along a constant-current device line occurs. At point c the frequency is approximately 100 MHz higher than that of point b. If the dc bias current is further increased, the frequency of oscillation will be increased along the circuit locus until point d is reached. At point d the stability criterion is not fulfilled which is similar to the case of point b. Beyond point d only wide-band noise was observed. This is expected since the loci of the device and circuit no longer intersect each other. Now if the tuning is reversed and the dc bias current is reduced, the frequency of oscillation will be decreased from points d to c and then to e. As the bias current is reduced along the locus of circuit towards point e, the RF voltage across the device is forced to approach its minimum. (This minimum RF voltage is approximately 3 V here. It can be calculated by using the actual

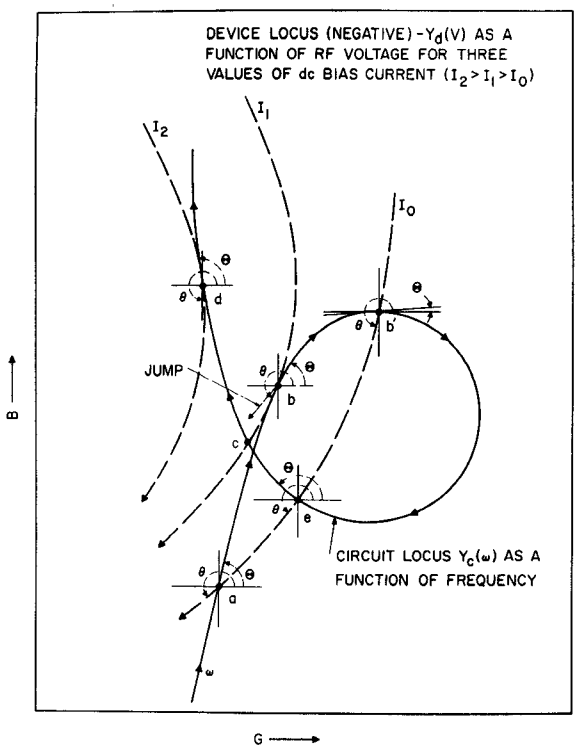

Fig. 7. Illustration of the stability criterion.

TABLE I

A SUMMARY OF THE STABILITY CONDITIONS FOR VARIOUS OPERATING POINTS IN FIG. 7

Point	$\frac{\partial G_d}{\partial V}$	$\frac{dG_c}{d\omega}$	$\tan\Theta - \tan\theta$	Stable
a	+	+	+	yes
b	+	+	0	no*
b'	+	+	−	no
c	+	−	−	yes
d	+	−	0	no*
e	+	−	−	yes

* At the threshold of instability.

circuit and device with a self-consistent analysis [15].) At point e, although both (1) and (2) are satisfied, the RF voltage falls below the sustaining voltage corresponding to the ac current flowing in the device and circuit. However, both (1) and (2) are satisfied for the same current level at point f but with the required RF voltage. Therefore, as the current level is reduced, a jump from point e to point f takes place and the oscillation is continued along the circuit locus from point f to point a as the dc current is further decreased. The details of the application of the oscillation and stability criteria to the above data are summarized in Fig. 7 and Table I.

It is interesting to point out that the nature of the jump from point b to point c differs from that of the jump from point e to point f. The former is due to the failure to satisfy the stability requirement and the latter, the self-consistent RF voltage requirement. Another interesting aspect in the observed data is that the slopes of the two continuous segments of frequency versus dc current curve (that is, curves a–b and e–d) in Fig. 5 are different. It is clear from Fig. 6 that this is due to 1) the unit frequency step (10 MHz) is not uniform along the locus of the circuit (i.e., the step in the segment a–b is smaller than that of the segment e–d), and 2) the relative angle which the loci of the circuit and device intersect each other in the two segments are different.

The slow increase of power observed in the experiment at the low current level is due to the fact that the locus of the circuit is almost parallel to the constant RF voltage line from point a to point b. Since the power is given by $(\frac{1}{2})V^2g$, where V and g are the RF voltage and negative conductance of the device at the operating point, respectively, the magnitude of the power is determined by the value of V when two points in the admittance plane are close to each other. The operating point which has a large value of V will have a higher power. This is the reason why the power after both jumps is higher than that before the jumps since, for both cases, the RF voltage is larger at the points after the jumps. The saturation of power at the high dc current level in the observed data (Fig. 5) is also due to this reason. Along the locus of the circuit from point c to point d in Fig. 6, due to the way the locus of the circuit is related to the constant RF voltage line, there is a point, before point d, where the RF voltage is a maximum and the power is peaked. Beyond this maximum RF voltage point, the RF voltage is decreased even though the dc bias current is increased. Therefore, the power is saturated beyond this point.

Temperature Effects: Several papers have presented experimental data on the variation of power and frequency of the IMPATT diode oscillator due to the change of junction temperature and have given qualitatively the theoretical basis of the dependence of the device admittance on temperature [16], [17]. Since mechanical tuning was performed for each data point, the effect of the circuit may be involved in these results considerably. In the present section experimental data is presented with the circuit effect minimized. No mechanical tuning is performed after an operating point is chosen. The main body of the coaxial cavity is held approximately at room temperature while the heat sink which is isolated thermally from it is kept at a constant temperature as the bias current is varied. This minimizes the variation of cavity dimensions with temperature. The change of output power and frequency with temperature can be considered mainly due to the change of device admittance with temperature.

The frequency and power of a free-running IMPATT diode oscillator as functions of dc bias current for a fixed external circuit are shown in Figs. 8(a) and (b), respectively, for four different values of heat sink temperature. In order to explain the observed data in terms of the device-circuit interaction, the admittances of the device and circuit will have to be superimposed on an admittance plane for each temperature. This is too lengthy to be presented here. Fortunately, a reasonably good explanation can be obtained by simply referring to the theoretical plot in Fig. 6.

The way that the frequency and power vary with temperature as shown in Fig. 8 is primarily due to the fact that at this operating point the magnitudes of the susceptance and the negative conductance of the device increase with the junction temperature. The precise manner in which they vary with temperature was not computed. At higher temperatures, when the heat sink is at 329 K and 290 K, respectively, in Fig. 8, there is a jump in both curves. This indicates that there is a loop in the circuit locus which first intersects the device line somewhere at 20 mA and the condition of oscillation and stability criterion continue to be satisfied until the

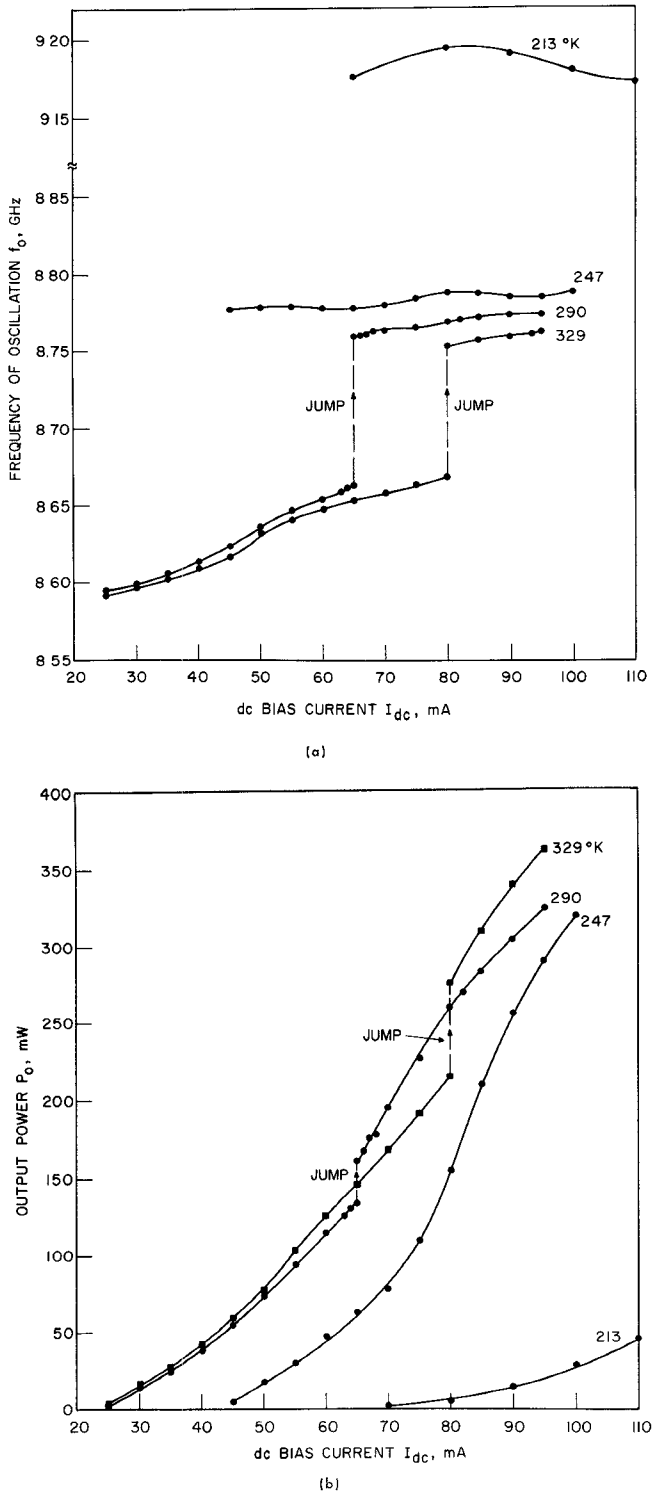

Fig. 8. Frequency of oscillation and output power versus dc bias current of an IMPATT diode oscillator for a fixed external circuit with the heat sink at four different temperatures. (a) Frequency. (b) Output power.

loop of the circuit admittance is tangent to the constant-current device line at 80 mA where a jump appears. The situation is similar to the path *a–b–c–d* in Fig. 6, except point *b* is now tangent to the constant-current device line at 80 mA. As the temperature is reduced, such as to a heat sink temperature of 290 K the magnitudes of the susceptance and negative conductance of the device decrease, and point *b* is now tangent to the device line at a lower current level of 65 mA. This

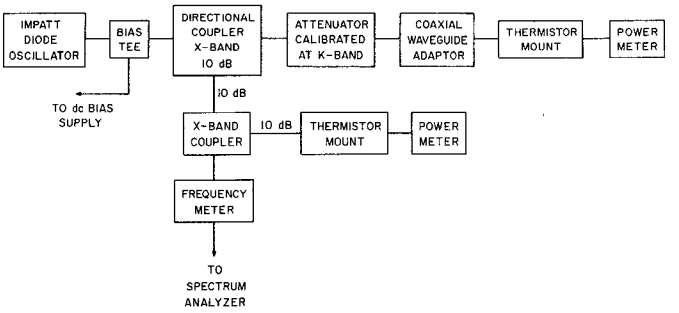

Fig. 9. Experimental setup used to measure the content of the second harmonic in an *X*-band IMPATT diode oscillator.

corresponds to the shift of the jump in the frequency and power for these two temperatures from 80 mA to 65 mA in Fig. 8. If the temperature is further reduced to a heat sink temperature of 247 K, more shift in the device admittance results and the loop in the circuit admittance does not intersect the device line. Therefore, no jump appears and the start-oscillation dc bias current level is higher since the upper tail of the loop of the circuit locus is able to intersect with the device line only at a current level higher than 40 mA. Further reduction in the temperature will only bring the device locus farther away from the loop of the circuit admittance. This is indeed confirmed by the data of the lowest heat sink temperature (213 K) which shows that the device does not oscillate until a dc current level as high as 70 mA is reached.

Harmonic Content: In this section, the results of the measurements on the harmonic content of a coaxial *X*-band IMPATT diode oscillator are presented. The experimental setup for measuring simultaneously the powers at the second harmonic and fundamental frequencies is shown in Fig. 9.

The output power and frequency of oscillation are measured through two miniature *X*-band 10-dB directional couplers and the power at the second harmonic is measured from the *K*-band port of the setup. The matching of the *K*-band output to the *X*-band circuit is taken care of by a broad-band fixed attenuator which is calibrated both at *X* and *K* bands.

The results are plotted in Figs. 10 and 11. In Fig. 10, the ratio of the fundamental and the second-harmonic powers is plotted against the frequency of oscillation with the current level as a parameter. The output power at the fundamental frequency is indicated at each data point. This figure shows that the content of the second harmonic varies from a maximum value of 12 dB to a minimum value of 40 dB below the fundamental output power. The value of the second harmonic has a maximum at 10.5 GHz and decreases above this frequency. In general, the content of the second harmonic is decreased with the frequency of oscillation above a certain frequency. The same data is plotted in Fig. 11. This figure shows that the higher the output power, the more the content of the second harmonic at each frequency.

Second-harmonic content can be minimized either by using an improved cavity design [18] or by operating the IMPATT diode at its second-harmonic null. It is expected from the theoretical considerations of the device physics [1] that a null in the second-harmonic content will occur when the transit angle through the device at the second-harmonic frequency is equal to 2π. For this case, reasonable power can be generated at the fundamental with relatively little second harmonic. This frequency is apparently higher than 12 GHz for the diodes used in these experiments. However, it is

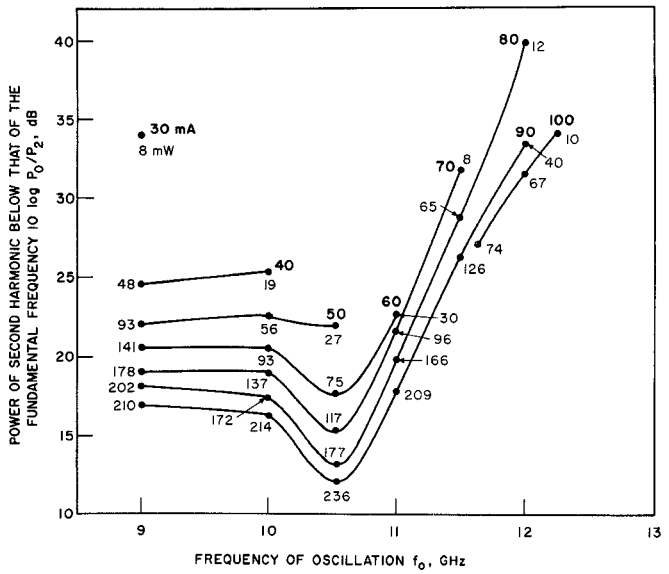

Fig. 10. Content of second harmonic versus frequency of oscillation for various dc bias current levels with output power P_0 indicated for each data point.

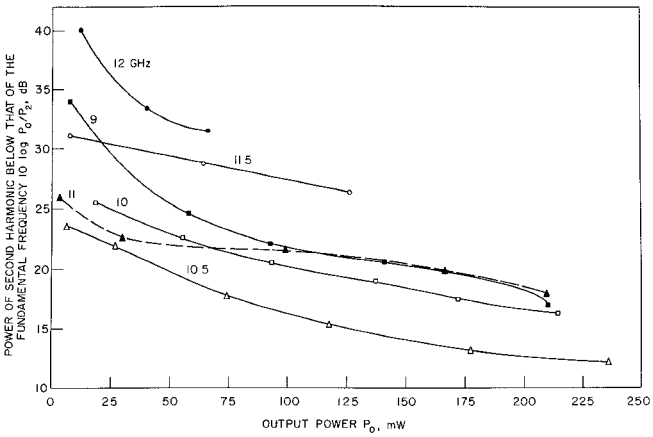

Fig. 11. Content of second harmonic versus output power for different frequencies of oscillation in X band.

evident from the results that the second-harmonic content is lower at higher frequencies even for the same power level at the fundamental.

Electronic Tuning Characteristics: Electronic tuning is greatly dependent on the operating point of the device as well as the external circuit. The experimental data in Fig. 12 illustrate this. The rate that the output power varies with the dc bias current may differ considerably with different operating points. It ranges approximately from a low rate of 4 mW/mA to a high rate of 18 mW/mA as calculated from the data in Fig. 12(a). In general, the frequency of oscillation of an IMPATT diode oscillator increases monotonically with the dc bias current for a fixed circuit condition [12]. However, this may not always be true, as shown in Fig. 12(b). The corresponding second-harmonic content in Fig. 12(c) also shows significant dependence on the circuit condition.

III. Behavior of a Bias-Modulated Oscillator

In this section the modulation properties of a bias-modulated IMPATT diode oscillator are presented. The experimental data with the operating point of the device chosen specifically to illustrate the significant effects of the operating point on

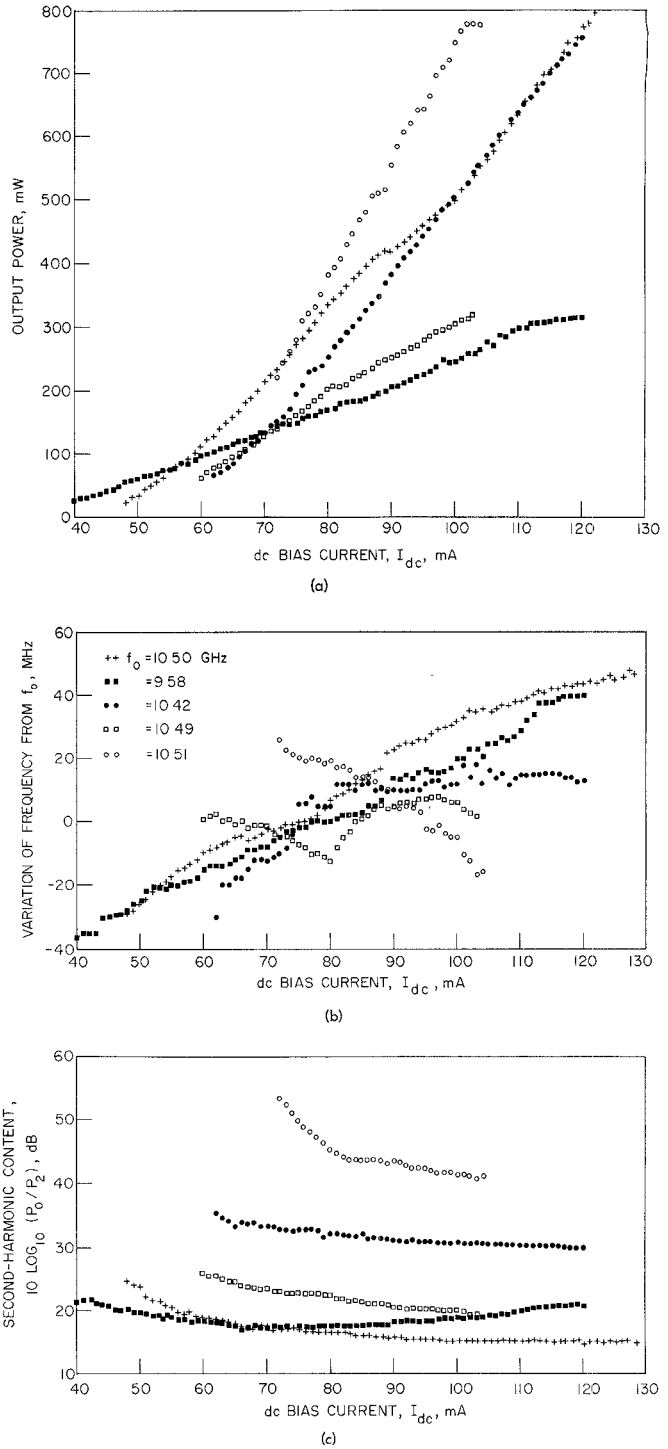

Fig. 12. Output power, frequency, and second-harmonic content of an IMPATT diode oscillator as functions of dc bias current for five different circuit conditions. (a) Output power. (b) Frequency of oscillation. (c) Second-harmonic content.

the modulation properties of the oscillator are presented and discussed. The effect of the effective Q_{ext}, which can be measured easily by the technique of injection locking, on the modulation properties of the bias-modulated IMPATT diode oscillator is discussed and compared with the theoretical expression, and good agreement is obtained. Experimental data for the FM and AM sensitivities as functions of modulation frequency for an arbitrarily chosen operating point of the device are studied and analyzed. Finally, experimental data showing the effect of injection locking on the AM and

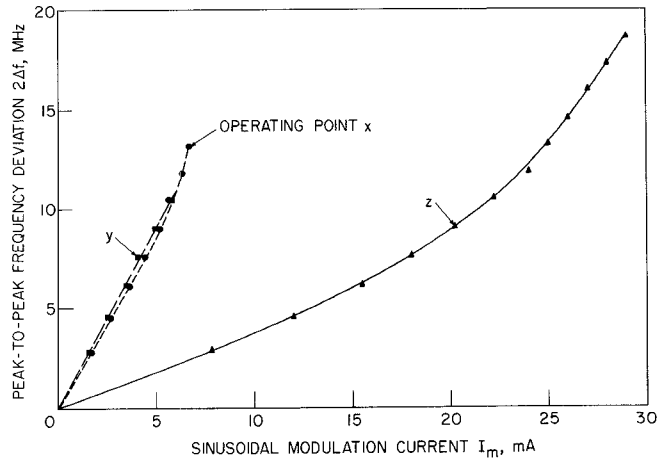

Fig. 13. Frequency deviation and percentage of amplitude modulation versus modulation current for three different operating points corresponding to points x and y in Fig. 5 and point z in Fig. 4 with modulation frequency at 600 kHz. (a) FM. (b) AM.

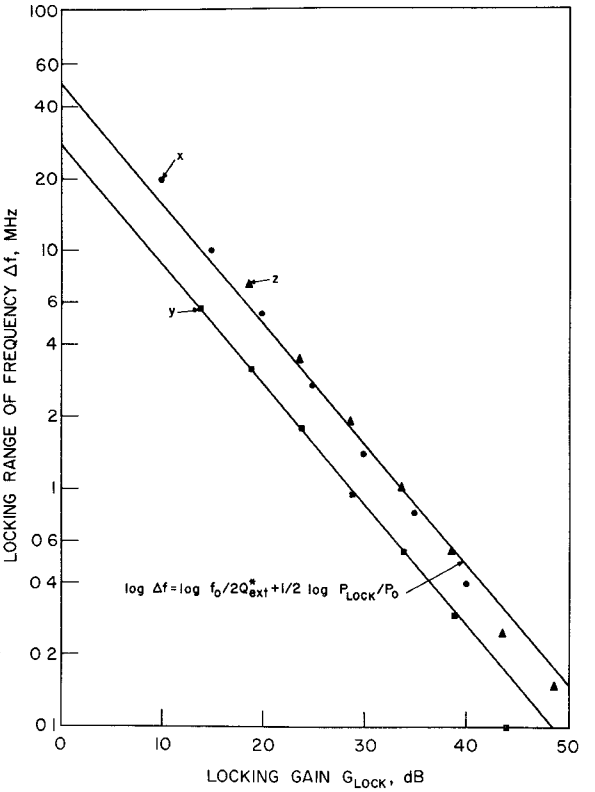

Fig. 14. Locking frequency range versus normalized injected signal power for three different operating points corresponding to points x and y in Fig. 5 and point z in Fig. 4.

FM sensitivities are presented. Again, emphasis is placed on the correlation of the experimental data with the theoretical development in terms of the device-circuit interaction.

A. Experimental Setup and Method

A low-frequency source and a 1-Ω resistor are connected to the bias network of the IMPATT diode oscillator through a capacitor to provide a source for modulation and to measure the value of the modulation current, respectively.

Frequency modulation is measured by the conventional Bessel null technique and amplitude modulation is measured by a crystal detector which is operated in its linear range.

B. Experimental Results and Discussion

Effect of the Operating Point: In order to illustrate the significant effect of the operating point on the modulation properties of a bias-modulated IMPATT diode oscillator, three operating points (points x and y in Fig. 5 and point z in Fig. 4) were chosen as operating points for bias-current modulation. They reveal distinct characteristics both in frequency and amplitude behavior when the oscillator is in the free-running condition. They are chosen in such a manner that they are in the middle of a continuous-frequency dc-current segment so that sufficient modulation current can be applied without having jumps occur in power and frequency or having the oscillator cease to oscillate.

The experimental data in Fig. 13 present the frequency and amplitude modulations as functions of the sinusoidal modulation current at a modulation frequency of 600 kHz for the three chosen operating points. Several features of the behavior of the free-running oscillator are shown in the modulation characteristic. First, point z of Fig. 4 which is selected in the middle of a long and continuous frequency-current segment allows a modulation current up to a peak value as high as 29 mA. On the other hand, points x and y of Fig. 5, which have comparatively shorter frequency-current segments due to the nonlinear behavior of the jump and hysteresis, allow a maximum modulation current of approximately 7 mA. In Fig. 4 an operating point at a dc bias current of 100 mA and an output power of 500 mW was selected to illustrate that an operating point which is near to the end of a frequency-current segment can have only a limited value of modulation current. The modulation properties of this point are similar to that of point z except that there is only a maximum allowable modulation current of 8 mA beyond which the oscillator breaks into noisy oscillation. (These data are not included here for lack of space.) Second, the expectation of low AM for operating point y in Fig. 5 which is chosen near a power saturation point is confirmed in Fig. 13(b) where there is less than 1 percent AM. Third, the experimental data of the locking frequency range versus locking gain for the three chosen operating points are shown in Fig. 14. Their operating conditions are shown in Table II. For the operating points x and z, which have almost the same values of Q_{ext}*, the latter has a smaller FM since the slope of its frequency-dc current curve in Fig. 4 is comparatively smaller. All these seem to suggest that there is a definite relationship between the modulation

TABLE II

OPERATING CONDITIONS FOR OPERATING POINTS x, y, AND z

Point	Output Power (mW)	Frequency (GHz)	Bias Current (mA)	dc Voltage (V)	Efficiency (percent)	Q_{ext}*
x	20	8.435	30	79	0.42	84
y	100	8.566	51.5	83	2.3	153
z	300	8.620	78.5	89	4.3	83

Note: Q_{ext}* is defined by the equation in Fig. 14 with the total locking range $2\Delta f$.

properties and the free-running behavior of the oscillator at a given operating point. However, the prediction of the modulation characteristic from the free-running oscillator behavior cannot be extended too far. In particular, the AM properties are not always predictable from its electronic tuning curve. For example, the maximum AM for operating point z is only 4 percent, surprisingly small for a modulation current of 29 mA. The corresponding free-running output power varies approximately from 30 mW to 570 mW for such a bias-current change when current is varied at a very slow rate. However, for a modulation frequency of 600 kHz, the situation is obviously quite different. There exists a nonlinearity which limits the AM when the modulation current is high. The precise mechanism of this nonlinearity is not known. It is probably due to the fact that the electronic tuning curve is only a static one and the modulation properties of a bias-modulated IMPATT diode oscillator are significantly influenced by the value of the impedance of the device at the modulation frequency which, in analogy to the RF case, can be a function of both the magnitude and frequency.

Effect of Q_{ext}:* Additional experimental data will be presented here to show that the FM property of a bias-modulated IMPATT diode oscillator depends significantly on the value of Q_{ext}*, while the AM is relatively insensitive to the value of Q_{ext}*. The relation between frequency deviation and Q_{ext} of an oscillator can be easily derived. A Taylor series expansion of the circuit reactance around the resonant frequency ω_0 in a lossless cavity and with the help of Foster's reactance theorem leads to

$$\frac{2\Delta f}{f_0} = -\frac{1}{Q_{ext}} \frac{\Delta X_d}{R_d}. \tag{3}$$

This means that the variation of frequency is inversely proportional to the magnitude of negative resistance and the external Q and is directly proportional to the variation of reactance ΔX_d of the device. Thus for a constant value of $\Delta X_d/R_d$, a smaller Q_{ext} gives a larger frequency modulation Δf. The experimental data which are designed to show the effect of Q_{ext} on the modulation properties of a bias-modulated IMPATT diode oscillator are shown in Fig. 15.

In Fig. 15 the peak-to-peak frequency deviation and percentage of amplitude modulation versus modulation current at a frequency of 600 kHz with the IMPATT diode oscillator biased at a constant dc current of 50 mA for three different operating points, which have almost the same output power but different values of Q_{ext}*, are shown. In Fig. 15(a) the slopes of the curves of frequency deviation versus modulation current, or the FM sensitivities, decrease with increasing Q_{ext}*. This result agrees well with the simple theoretical expression given in (3). It is reasonable to assume that the value of $\Delta X_d/R_d$ for each operating point is approximately the same since an examination of computer calculations of the device impedance, which is similar to that of Fig. 3 except at a dc bias current of 50 mA, indicates that the locus of the device is quite uniform in the region of interest and that the value of $\Delta X_d/R_d$ for each of the operating points in Fig. 15 can be taken to be equal. The corresponding AM properties shown in Fig. 15(b) indicate no dependence on Q_{ext}*. This is as expected from theoretical considerations. It is interesting to point out that the nonlinearity again comes into the picture at a high modulation current and limits the AM to a maximum of 7 percent. This is not observed for the low-level modulation [19].

FM and AM Sensitivities: All the experimental data presented so far for the modulation of a bias-modulated IMPATT diode oscillator were taken at a modulation frequency of 600 kHz. This value of modulation frequency was chosen arbitrarily but is fixed so that distinct modulation properties due to different operating points and Q_{ext} can be determined. From these results it is clear that a comparison of AM and FM sensitivities at different oscillation frequencies for a fixed modulation frequency and bias current are not meaningful unless additional parameters such as the external Q and the electronic tuning characteristic of the IMPATT diode oscillator are specified. In this section the effects of varying the modulation frequency on the modulation properties of a bias-modulated oscillator at an arbitrarily chosen operating point are presented.

The experimental results for FM and AM sensitivities as functions of the modulation frequency at a given operating point are shown in Fig. 16. The method for these measurements is the same as for all the data presented except that each data point in Fig. 16 represents the slope of a series of AM and FM data versus modulation current. The decrease of AM sensitivity with the modulation frequency at higher modulation frequencies and the gradual increase of FM sensitivity with the modulation frequency agree qualitatively with the simple theoretical results presented elsewhere [20]. The experimental data in Fig. 16 give a typical indication that the variation of FM and AM sensitivities with the modulation frequency depends on the impedance of the device and circuit at both the microwave and modulation frequencies. The level of these curves may depend primarily on the operating point of the device but their shapes depend on the value of the impedance of the circuit and device at the modulation frequency. Therefore, a properly designed bias network to give an appropriate low-frequency impedance is important.

Effect of Injection Locking on the Modulation Properties: In order to illustrate the effect of a locking signal on the modulation sensitivities, the free-running oscillator was first bias modulated by a modulating frequency of 1 MHz and its output power at the fundamental frequency (or carrier) was nulled at a modulation current of 1.5 mA. The external locking signal which is set at the free-running oscillator frequency is then injected into the oscillator with the modulation current and frequency held constant. The magnitude of the carrier as compared to that of the sideband is increased with the level of injected signal power. The results are shown in Fig. 17 where it is seen that the FM and AM sensitivities are reduced as the level of the injected signal power is increased. The locked and bias-modulated IMPATT diode oscillator becomes unlocked

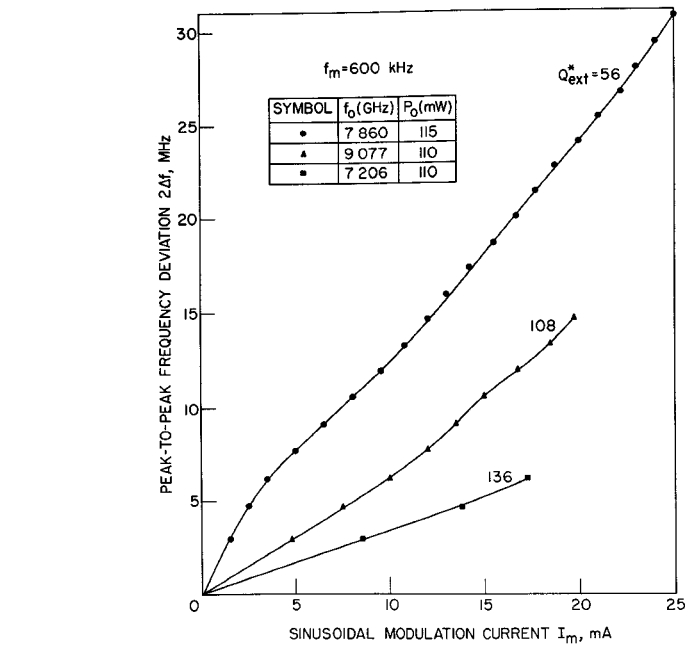

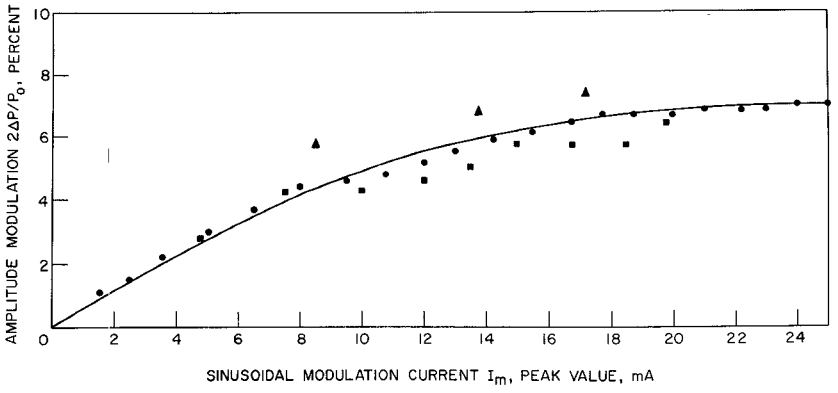

Fig. 15. Frequency modulation and percentage of amplitude modulation versus modulation current with the IMPATT diode oscillator biased at a constant dc current of 50 mA for three different operating points which have almost the same output power but different values of effective external Q, Q_{ext}*. (a) FM. (b) AM.

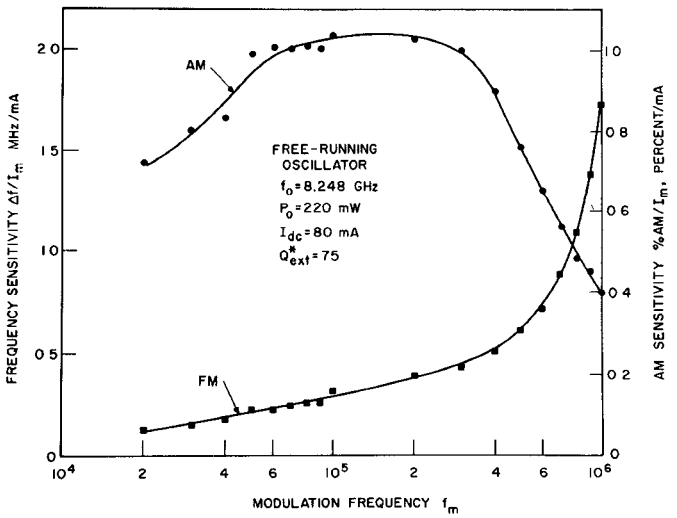

Fig. 16. FM and AM sensitivities versus modulation frequency.

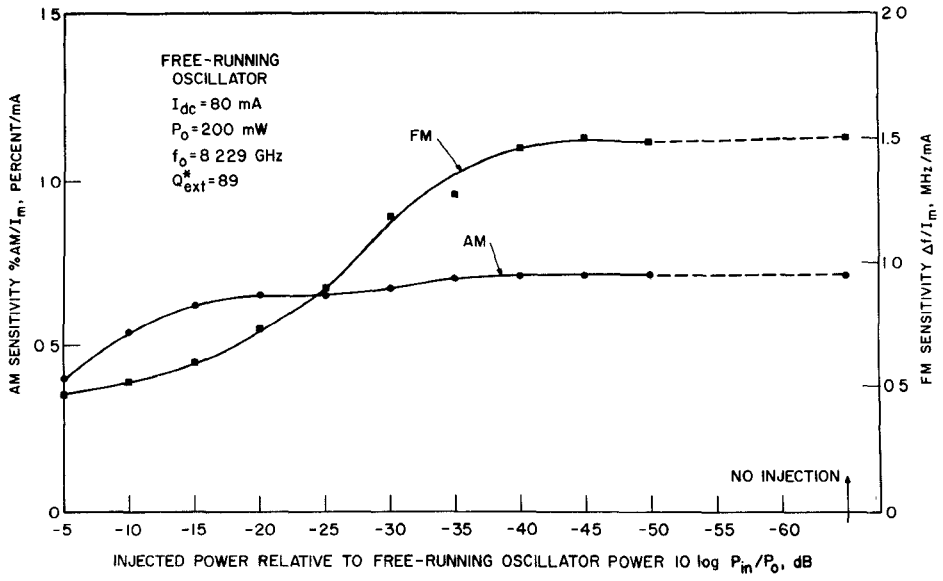

Fig. 17. FM and AM sensitivities as functions of the injected power level for the injected signal frequency at the free-running oscillator frequency. (Modulation frequency $f_m = 1$ MHz and modulation current $I_m = 1.5$ mA.)

when the locking signal is very low. This is apparently due to the fact that the frequency deviation caused by the modulation exceeds the locking frequency range. This is shown by the dashed line on the right-hand portion of the curve in Fig. 17.

IV. Conclusions

Stable oscillation of a negative-conductance diode oscillator can be obtained only if the conditions for oscillation and stability are fulfilled simultaneously at an operating point of the oscillator. Since the theoretical calculation of the device admittance indicates that a negative conductance exists for a wide range of frequency, the reason for failing to oscillate at a desired frequency in this range is quite often due to the inadequacy of the value of the circuit admittance. The jump and hysteresis in frequency and power as functions of the dc bias current of a free-running IMPATT diode oscillator observed experimentally were analyzed theoretically in a complex plane on which the admittances of the device and circuit corresponding to actual experimental conditions are superimposed. The reason for such nonlinear phenomena is due to the combined effects that a loop exists in the circuit locus which overlaps partially with the device locus, the requirements of the conditions for oscillation and stability and the requirement of the self-consistent RF voltage. The effect of temperature on the device is to vary the admittance of the device. The change of the power and frequency of the oscillator due to different heat sink temperatures observed experimentally can be explained as the shifting of the operating point of the device in terms of the device-circuit interaction. The content of the second harmonic in a coaxial IMPATT diode oscillator for the diodes used in these experiments is decreased with the frequency of oscillation above a certain frequency. The higher the output power at the fundamental, the more the content of the second harmonic at each frequency. Second-harmonic content can be minimized either by using an improved cavity design or by operating the IMPATT diode at its second-harmonic null.

The modulation properties of a bias-modulated IMPATT diode oscillator depend on its operating point. A knowledge of the free-running behavior of the oscillator at and near a given operating point, such as the electronic tuning curve, and a value of the effective Q_{ext} are important for the prediction of its modulation properties at this operating point.

References

[1] G. I. Haddad, P. T. Greiling, and W. E. Schroeder, "Basic principles and properties of avalanche transit-time devices," *IEEE Trans. Microwave Theory Tech. (Special Issue on Microwave Circuit Aspects of Avalanche-Diode and Transferred Electron Devices)*, vol. MTT-18, pp. 752–772, Nov. 1970.

[2] S. M. Sze and R. M. Ryder, "Microwave avalanche diodes," *Proc. IEEE (Special Issue on Microwave Semiconductors)*, vol. 59, pp. 1140–1154, Aug. 1971.

[3] W. E. Schroeder and G. I. Haddad, "Nonlinear properties of IMPATT devices," *Proc. IEEE*, vol. 61, pp. 153–182, Feb. 1973.

[4] M. E. Hines, "Large-signal noise, frequency conversion, and parametric instabilities in IMPATT diode networks," *Proc. IEEE*, vol. 60, pp. 1534–1548, Dec. 1972.

[5] C. A. Brackett, "The elimination of tuning-induced burnout and bias-circuit oscillations in IMPATT oscillators," *Bell Syst. Tech. J.*, vol. 52, pp. 271–306, Mar. 1973.

[6] K. Kurokawa, "Some basic characteristics of broadband negative resistance oscillator circuits," *Bell Syst. Tech. J.*, vol. 48, pp. 1937–1955, July 1969.

[7] N. D. Kenyon, "A lumped-circuit study of basic oscillator behavior," *Bell Syst. Tech. J.*, vol. 49, pp. 255–272, Feb. 1970.

[8] J. L. Blue, "Approximate large-signal analysis of IMPATT oscillators," *Bell Syst. Tech. J.*, vol. 48, pp. 383–396, Feb. 1969.

[9] W. E. Schroeder and G. I. Haddad, "Effect of harmonic and subharmonic signals on avalanche-diode oscillator performance," *IEEE Trans. Microwave Theory Tech.* (Corresp.), vol. MTT-18, pp. 327–331, June 1970.

[10] C. Y. Duh and J. L. Moll, "Electron drift velocity in avalanching silicon diodes," *IEEE Trans. Electron Devices*, vol. ED-14, pp. 46–49, Jan. 1967.

[11] C. R. Crowell and S. M. Sze, "Temperature dependence of avalanche multiplication in semiconductors," *Appl. Phys. Lett.*, vol. 9, pp. 242–244, Sept. 1966.

[12] M. Gilden and M. E. Hines, "Electronic tuning effects in the Read microwave avalanche diode," *IEEE Trans. Electron Devices*, vol. ED-13, pp. 169–175, Jan. 1966.

[13] I. W. Pence, Jr., "Impedance of packaged Gunn diode and parametric circuit application," Ph.D. dissertation, Univ. Mich., Ann Arbor, 1970.

[14] P. I. Somlo, "The computation of coaxial line step capacitances," *IEEE Trans. Microwave Theory Tech.*, vol. MTT-15, pp. 48–53, Jan. 1967.

[15] M. S. Gupta and R. J. Lomax, "A self-consistent large-signal analysis of a Read-type IMPATT diode oscillator," *IEEE Trans. Electron Devices*, vol. ED-18, pp. 544–550, Aug. 1971.

[16] W. E. Schroeder and G. I. Haddad, "The effect of temperature on the operation of an IMPATT diode," *Proc. IEEE (Special Issue on Microwave Semiconductors)* (Lett.), vol. 59, pp. 1242–1244, Aug. 1971.

[17] W. J. Chudobiak, R. McKillican, and V. Makios, "The effect of junction temperature on the output power of a silicon IMPATT diode," *Proc. IEEE* (Lett.), vol. 60, pp. 340–341, Mar. 1972.
[18] C. A. Brackett, "Characterization of second-harmonic effects in IMPATT diodes," *Bell Syst. Tech. J.*, vol. 49, pp. 1777–1810, Oct. 1970.
[19] J. W. Amoss and K. E. Gsteiger, "Frequency modulation of avalanche transit time oscillators," *IEEE Trans. Microwave Theory Tech. (1967 Symposium Issue)*, vol. MTT-15, pp. 742–747, Dec. 1967.
[20] G. Weidmann, "Amplitude and frequency modulation sensitivity of IMPATT diode oscillators," *Nachrichtentech. Z.*, vol. 23, pp. 368–371, July 1970.

Short Papers

Waveguide and Stripline 4-Port Single-Junction Circulators

J. HELSZAJN

***Abstract*—The modal and eigenvalue approaches of 4-port single-junction circulators are combined to describe the theory and construction of a waveguide device and a stripline device. The three independent variables used in the case of the waveguide one are a pair of $HE_{\pm1,1,1}$ open dielectric resonances in a demagnetized ferrite disk, a $TM_{0,1,1}$ resonance on a metal post, and the magnitude of a direct field to remove the degeneracy between the $HE_{\pm1,1,1}$ modes. The eigenvalue approach is used to establish systematically each condition one at a time. The variables used in the construction of the stripline junction are a pair of radial $n=\pm3$ degenerate resonances, a radial $n=0$ resonance, and the amplitude of a direct field to split the degeneracy between the former modes. In this case a circulation condition is found in which it is possible to omit one of the circulation adjustments.**

Introduction

The 4-port H-plane waveguide circulator described in this short paper consists of a single magnetized ferrite disk on one side of the waveguide and a metal post on the other wall. A similar arrangement has been used experimentally before but with the ferrite and the metal posts each half the height of the waveguide [1]. The three variables in this last geometry were the diameters of the ferrite and metal posts and the direct magnetic field. In the light of some recent work a more appropriate mode nomenclature for circulation in this type of geometry is in terms of higher order $HE_{\pm1,1,n}$ resonances [2]. In the present geometry the three junction modes are identified as a pair of hybrid $HE_{\pm1,1,1}$ open dielectric resonant ones along the demagnetized ferrite disk and a single symmetrical resonant one associated with a quarter-wave-long thin metal post. The exact shape of the ferrite disk is here determined by the boundary conditions of an open dielectric $HE_{\pm1,1,1}$ resonator [3]. The length of the metal post is approximately a quarter-wave in free space [2], [4], [5]. Such a metal post has also been used in the construction of 3- and 4-port waveguide circulators [6], [7]. Since the overall length of the ferrite disk and the quarter-wave-long cylinder are approximately equal to the height of the waveguide, the two cylinders are here also allowed to make firm flat contact with each other and with the waveguide walls [1]. These two boundary conditions satisfy two of the three independent variables of the junction. The third and last one is satisfied by magnetizing the junction with an appropriate direct magnetic field thereby rotating the standing wave formed by the hybrid $HE_{\pm1,1,1}$ modes by the required 45°.

The procedure used to adjust this circulator is the one described in [7] and [8]. It allows each of the three independent variables for this type of junction to be established one at a time in a systematic way.

This short paper also includes the theory and construction of a 4-port single-junction stripline circulator. The modes used in the construction of this one have nearly equal radial wavenumbers. This means that a simple ferrite disk immediately satisfies the first two out of the three circulation conditions for this type of junction. The third and last one is obtained in the usual way by removing the degeneracy between the degenerate modes by biasing the junction with a direct magnetic field. The field patterns used in this case are the $n=0$ mode and the $n=\pm3$ modes with $H_\phi=0$ at $r=R$ in a simple disk with no variation of the electric field along the disk axis.

Additional references to the literature of 4-port single-junction circulators may be found in [9]–[14].

Manuscript received August 1, 1972; revised March 26, 1973.
The author is with the Department of Electrical and Electronic Engineering, Heriot-Watt University, Edinburgh, Scotland.

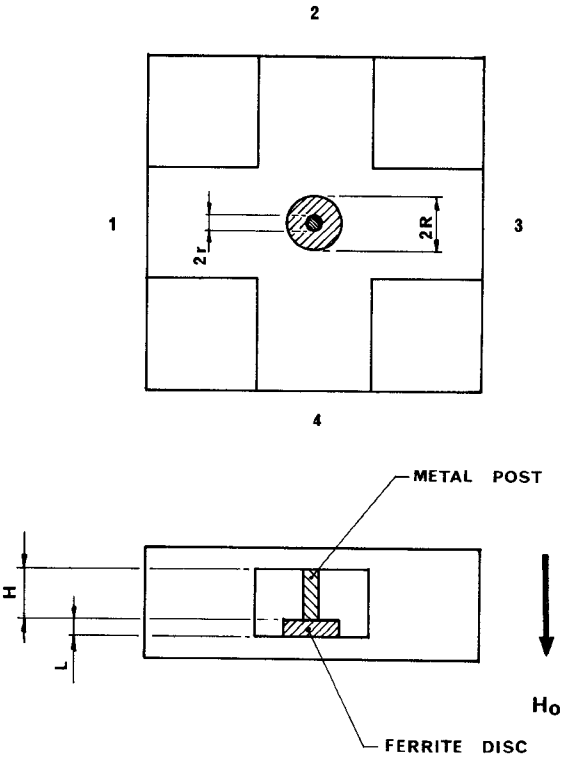

Fig. 1. Schematic of single-junction 4-port waveguide circulator.

4-Port Single-Junction Circulator Using Axial Modes

The 4-port single-junction circulator described in this short paper relies on a linear combination of $HE_{\pm1,1,1}$ and $TM_{0,1,1}$ axial modes for its operation. Once these modes are resonant within the junction the $HE_{\pm1,1,1}$ one is rotated by the application of a direct magnetic field to form a circulator. The geometry considered here is shown in Fig. 1.

The field patterns employed here are shown in Fig. 2(a)–(d). The illustrations in Fig. 2(a) and (b) show the $HE_{\pm1,1,1}$ and $TM_{0,1,1}$ modes